Novel Polymer and Peptide REACTION-based Theranostics for MRI.

Laura Szkolar Sienkiewicz[1], Dorela Shuboni-Mulligan[1], Christiane Mallett[1], and Erik Shapiro[1]

[1]*Radiology, Michigan State University, East Lansing, MI, United States*

Synopsis

MRI offers a unique opportunity for theranostic agent development. By engineering both polymer and peptide materials, we have scope to successfully target, image and treat a range of biological conditions. Here we successfully demonstrate the use of targeted and triggered nanoparticles, encapsulating imaging and chemotherapeutic agents, as theranostics for MRI.

INTRODUCTION:

REACTION[1] (release activated iron oxide nanoparticle) based theranostic agents release their encapsulated nanocrystal/therapeutic payload upon enzymatic cleavage, turning on MRI contrast at the site of activation and delivering therapeutics only locally.

The use of environmentally sensitive materials for targeted dual imaging-treatment agents offers an attractive alternative to a range of conventional therapies[2]. The encapsulation of cytotoxic agents, such as doxorubicin (DOX), can improve treatment efficacy, whilst limiting dose-related toxicity[3].

Peptide and biopolymer materials offer new scope for fabricating novel theranostic agents[4]. Enzyme-specific structural motifs can be engineered for catabolism by local enzymes, many of which are secreted as the result of a biological event, such as tumor metastasis[5]. Targeting molecular events in this way offers a new mode of biological imaging and personalized medicine.

Herein we present polymer and peptide encapsulated iron oxide (Fe_3O_4) and DOX nanoparticles, for enzymatically activated MRI theranostic agents. Intact nanoparticles encapsulate hydrophobic payloads, excluding water from experiencing high magnetic susceptibility gradients[6], quenching their relaxivity and inhibiting the release of drug. Upon enzymatic degradation, the magnetic payload is released, increasing relaxivity and turning the agent 'on' whilst offering simultaneous therapeutic release.

METHODS:

Cellulose nanoparticles encapsulating Fe_3O_4 nanocrystals (10mg/mL,25%w/w Fe_3O_4) and fluorescent coumarin-6 were fabricated as previously reported[7,8]. VPVG21 and VPVG23 peptide, with MMP recognition sites, spontaneously self-assembled to form nanoparticles in dH_20 (5mg/mL,25% w/w Fe_3O_4, DOX 4%w/w) before snap freezing and lyophilizing. Elastase and cellulase were conjugated with Texas Red for fluorescence microscopy. Nanoparticle formation and diameter were measured by SEM and DLS. Stability in buffer and iron content was measured using ICP. DOX nanoparticle stability and loading capacity was calculated *via* measurements at 480nm.To demonstrate internalization primary rMSCs were labelled with nanoparticles and incubated (0.1 mg/mL,24hours). Confocal microscopy and CryoTEM were used to show particle location within the rMSCs, and cytotoxicity was assessed using an MTT assay. Particle degradation was visualized *via* SEM. Change in relaxivity(r_2^*) was measured at 7T *via* T_2^* measurements using a multi-gradient echo sequence. SD rats received bilateral intracranial injections of labelled rMSCs and were imaged *via* MRI. Subsequent ICP was performed on cell samples to show iron content.

RESULTS:

Peptide and cellulose nanoparticles were highly spherical (Figure 1a-f). Cellulose particles (Figure 1g) had larger diameters (c.a. 250-500nm) when compared with their peptide (Figure 1h) counterparts (170-300nm). Particles demonstrated loading of ~25% Fe_3O_4/65% DOX (Figure 2) and TEM further demonstrated the successful encapsulation of hydrophobic payloads (Figure 1a-c inset).

Upon incubation with rMSCs, nanoparticles were internalized (Figure 3a) into the lysosome (Figure 3b). Nanoparticles were stable in buffer (Figure 3c) allowing high viability for labelled rMSCs (Figure 3d). Upon addition of the matching enzyme however, particle release of DOX resulted in cell death (Figure 3d).

T_2^* measurements demonstrated a significant change in contrast upon addition of the matching enzyme (Figure 4a,b), resulting in a ~3 fold change in relaxivity (Figure 4c). Here the relaxivity mediation is a direct result of the removal of particle degradation (Figure 4d). The same phenomenon was successfully demonstrated *in vivo* (Figure 5a-c) where labelled cells resulted in little contrast. Upon the addition of enzyme, relaxivity increased and the cells were visualized (Figure 5d). Iron content in both cellular injections was equivalent (Figure 5e).

DISCUSSION:

We demonstrate that biopolymer and peptide nanoparticles are suitable for the encapsulation and enzymatically triggered release of hydrophobic payloads.

All particle types were subject to enzymatic coat degradation, where successful coat removal resulted in a significant modulation of relaxivity and increased targeted cell death. A key limitation to the use of nanoparticles as MRI theranostic agents is the ability to "switch the agent on" only under the correct conditions. The use of enzymes secreted only in specific biological events, such as MMP's, or by use of lysosomal pH specific enzymes allows an avenue by which release can be controlled.

No previously reported *in vivo* studies have successfully demonstrated a clear difference in contrast as a result of enzymatic coat removal. In all rats imaged, a large difference in contrast was seen, despite the presence of similar levels of iron oxide. This, along with the excellent biocompatibility and long-lived biodegradation makes them highly suitable candidates for MRI theranostic agents.

CONCLUSION:

The successful production of an enzymatically switchable nanoparticle offers significant scope for highly targeted imaging and drug delivery utilizing MRI.

The large change in contrast, as a result of the triggered degradation of the particle, allows for the visualization of cellular events and targeted therapy *in vivo*. The use of peptides particularly offers scope for *de novo* design of a multitude of enzyme specific particles.

Acknowledgements

Financial support from NIH R21 EB017881 is greatly appreciated.

References

[1] Granot, D. Shapiro, EM. Release activation of iron oxide nanoparticles: (REACTION) A novel environmentally sensitive MRI paradigm. Magnetic resonance in medicine. 65;5(2011):1253–1259

[2] Chun Li, A targeted approach to cancer imaging and therapy, Nature Materials. 2014;13:110–115

[3] Chen YC, Bathula SR, Li J, Huang L. Multifunctional nanoparticles delivering small interfering RNA and doxorubicin overcome drug resistance in cancer. J. Biol. Chem. 2010; 285:22639–22650

[4] Goldberg, M. J Biomat Sci. Nanostructured materials for applications in drug delivery and tissue engineering. 2007;18(3): 241-268

[5] Hussein D Foda, Stanley Zucker, Matrix metalloproteinases in cancer invasion, metastasis and angiogenesis, Drug Discovery Today, Volume 6, Issue 9, 1 May 2001, Pages 478-482

[6] Tóth, E. Helm, L. Merbach, AE. Relaxivity of MRI Contrast Agents. Contrast agents I: topics in current chemistry. 221 (2002): 61-101

[7] Park J. Hyeon T. Synthesis of monodisperse spherical nanocrystals. Angewandte Chemie International Edition. 46(2007):4630-4660

[8] Nkansah, MK. Thakral, D. Shapiro, EM. Magnetic poly(lactide-co-glycolide) and cellulose particles for MRI-based cell tracking. Magnetic resonance in medicine. 65; 6(2011):1776–1785

Figures

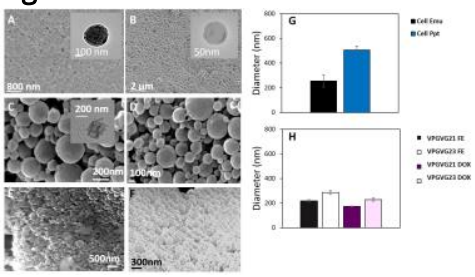

Figure 1. Characterization *via* SEM of a) cellulose-FE emulsion, b) cellulose-FE nanoprecipitation, c) VPGVG-21-FE, d) VPGVG-23-FE, e) VPGVG-21 DOX and f) VPGVG-23-DOX nanoparticles and DLS analysis of g) cellulose and h) peptide nanoparticles.

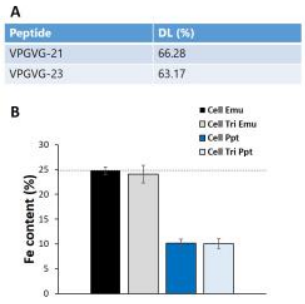

Figure 2. The loading capacity (DL) of a) DOX in VPGVG-21 and VPGVG-23 and b) ICP data of encapsulated iron concentration in Cellulose nanoparticles. Where data point represents mean, error bars ±SD.

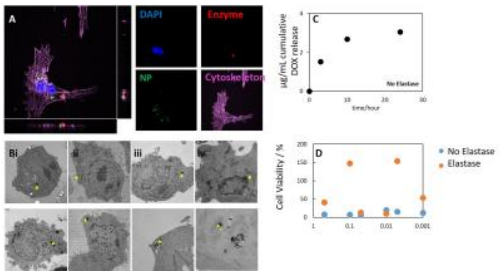

Figure 3. a) Confocal imaging of the cellular uptake of nanoparticles within primary MSCs after 24 hours incubation, where the cytoskeleton is visualized in purple, nuclei in blue, nanoparticles green and enzyme red b) Cell-TEM images showing iron internalization within primary mesenchymal stem cells after incubation with 0.1 mg/mL cellulose nanoparticles at i) 30 min ii) 1h iii) 3h and iv) 24 hours (pH 7,37°C,5% CO_2) c) the

cumulative release of DOX from VPGVG-21 nanoparticles incubated in PBS without elastase (30h) and d) MTT assay demonstrating the difference in cell viability as a result of elastase particle degradation.

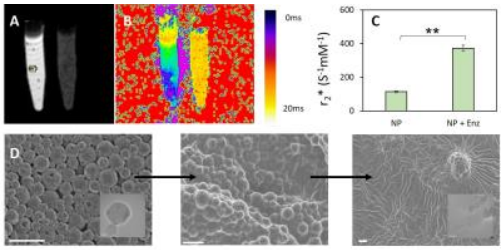

Figure 4. a,b) MRI analysis of the effect of cellulase incubation with Cellulose nanoparticles after 24 hours incubation (37^{o}C,pH 5.5) c) The relaxivity (r_2^*) versus concentration for the same systems and d) SEM images demonstrating particle degradation. Where MRI scan parameters were: T_2^* multi-gradient echo sequence resolution 400x400 um, slice thickness 1 mm. Where data point represents mean, error bars ±SD.

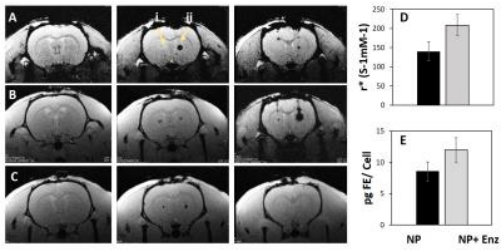

Figure 5. *In vivo* introduction of Cellulose nanoparticles using a-c) MRI of primary rMSCs 0 days post-bilateral intracranial injection, where i) received administration of nanoparticles alone and ii) received nanoparticles and cellulase, d) quantification of the change in relaxivity (r_2^*), as a result of enzyme presence *in vivo* and e) the quantification of iron present, *via* ICP, within those cell suspensions administered. Where data point represents mean, error bars ±SD.